Simulation of Ceramic Particle Formation: Comparison with *in-situ* Measurements

Ceramic particle formation processes have been studied using SiO_2 as a model compound. Silica particles have been synthesized in a counterpropagating diffusion flame reactor, in which *in-situ* measurements of particle size and number density have been made. In addition, the time-temperature history of the particle field has been calculated from a flame simulation. Numerical simulations using moment and sectional methods for particle formation have been applied and compared to the experimental measurements. The simulations for the particle formation assume a kinetically-constrained approach, allowing a simple representation of nucleation, surface growth and coagulation. The results suggest that, if the source rates are known well enough, particle formation of low vapor pressure species can be predicted. Both models do well in predicting the gross features of particle formation (number density and mean particle size), although the moment solution does a poor job of predicting the polydispersity effects during periods of high monomer generation rates.

M. R. Zachariah
H. G. Semerjian
Center for Chemical Technology
National Institute of Standards and Technology
Gaithersburg, MD 20899

Introduction

The production of submicron powders is an area that has been identified as key to the future expansion in applications of ceramic materials (Sanders, 1984). Recent advances in ceramic science have led to greater interest in improving the processing techniques for this class of materials. The major goals are the production of spherical, unagglomerated submicron particles of well-characterized and controlled size distribution, with the requisite chemical structure. Success is dependent heavily on the methods chosen and the processing conditions used. A variety of aerosol processing methods are currently being investigated which include laser synthesis (Cannon et al., 1982), plasma (Girshick et al., 1988), thermal (Alam and Flagan, 1986), and flame methods (Ulrich, 1984; Ulrich and Subranmanian, 1977; Chung and Katz, 1985; Zachariah et al., 1989, in press).

Each method provides its own set of advantages, the choice depends on the desired product and its characteristics. Flames have historically been viewed almost exclusively as energy generators, although more recently they are being seen as a unique environment for chemical synthesis. Exploitation of this environment requires understanding the dynamics of flames, as well as the fundamentals of particle formation and growth of these materials. This paper describes the simulation of particle formation in flames and compares the results from *in-situ* measurements of particle size and number density. We selected to study silica particle formation, since it is an industrially-important aerosol and serves as a generic species for investigation of refractory particle formation processes.

Experimental Studies

Studies on the formation of silica particles have been conducted in a counter-propagating diffusion flame as first described by Chung and Katz (1985). The reactor consists of two counterflowing rectangular brass ducts separated by a distance of 15 mm. The flow field is constrained to two dimensions with fused silica windows placed on the sides of the smaller cross-sectional dimension of the duct. Previous studies in this reactor by Zachariah et al. (1989) and Zachariah et al (in press) dealt with the diagnostic techniques used and the growth characteristics found. Both dynamic light scattering and angular dissymmetry methods were employed to obtain *in-situ* measurements of particle size and number density in the counterpropagating hydrogen-oxygen diffusion flame shown in Figure 1. For these studies, silica was produced by doping small quantities of silane (less than 0.5 mol %) in the hydrogen stream. Particles are formed and grow as they flow toward the stagnation plane where they are swept out of the reactor. The advantage of this geometry is that, along the stagnation point streamline, the flow may be

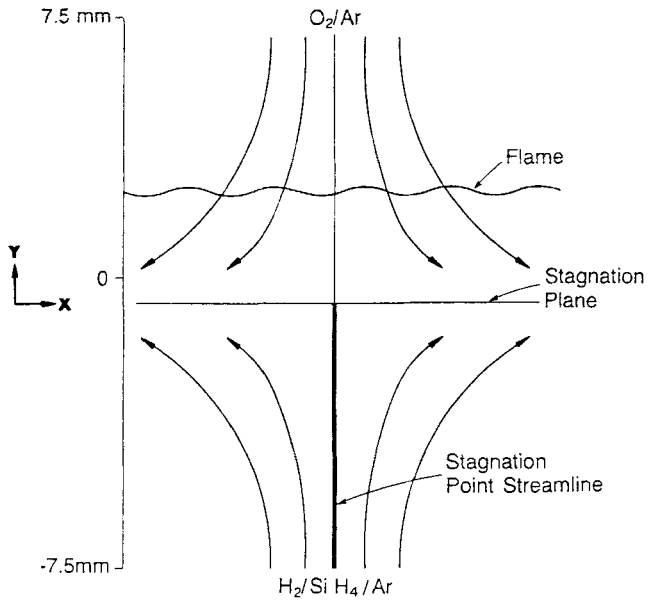

Figure 1. Counterflow diffusion flame flow field.
The dark line, corresponding to the stagnation point streamline, marks the region probed by the laser.

treated as one-dimensional, greatly reducing the number of measurements required and providing a much more tractable geometry to model than the more-commonly encountered 2-D diffusion flames.

The diagnostic technique used for the measurement of particle size and number density was light scattering dyssymmetry, as illustrated in Figure 2 and described in detail elsewhere

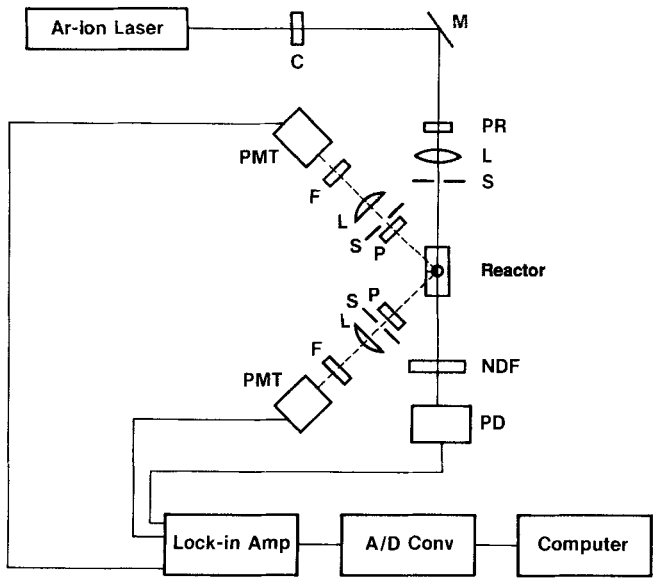

Figure 2. Scattering dissymmetry measurement system.

C = chopper	P = polarizer
M = mirror	F = narrow bandfilter
PR = polarization rotator	PMT = photomultiplier
L = lens	NDF = neutral density filter
S = spatial filter	PD = photodiode

(Zachariah et al., 1989). The diagnostic relies on measuring the anisotropy of scattered light from particles in the Mie size range ($\pi d/\lambda > 0.3$). Where d is the diameter of the scatterer and λ is the wavelength of light. In brief, a 4-W argon ion laser operating at the 514.5 nm line was mechanically chopped at 1,018 Hz. Because of the steep gradients in temperature and species, the beam was focused with a 500-mm lens to provide an axial resolution of 0.2 mm. The laser beam polarization was maintained perpendicular to the scattering plane and vertically polarized scattered light at 45° and 135° from the forward scattering angle was monitored with photomultipliers. In addition, the transmitted laser intensity was monitored with a photodiode. The three data channels were collected by standard phase-sensitive detection methods (see Figure 2). The data reduction to obtain particle size and number density was based on Mie theory assuming a log-normal self-preserving size distribution. Temperature measurements were obtained using butt-welded 125-μm Pt/Pt-10% Rh thermocouples (ceramic coated to prevent radical recombination) corrected for radiation losses or alternately from Laser-induced fluorescence measurements of two rotational lines of the OH radical.

The results obtained showed that the two most important process variables influencing particle growth and morphology were precursor concentration (silane) and temperature. Silane concentration was found to be the primary particle-size-determining variable, affecting the mechanism of growth from one of nucleation-coagulation growth at low levels of silane concentration (mole fraction in fuel < 0.01 mol %) to one of surface condensation-coagulation at the higher silane concentrations. Temperature effects were also seen to affect the mechanism of growth to a more nucleation-dominant mechanism as the temperature in the flame was increased, resulting in a larger number density of smaller particles. More importantly, the increased temperature was seen to dramatically effect particle morphology by sintering the agglomerates into highly spherical structures.

Time-Temperature History and Source Rates

In order to account for the various stages of particle formation and growth, a knowledge of the flow field in the counterpropagating flow is required, as well as the rate at which the SiO_2 monomer is formed. The flow field was calculated using the formalism of Smooke (Smooke et al., 1986). The governing boundary layer equations for mass, momentum and chemical species may be expressed in the following form when a similarity solution is assumed for the two components of velocity; $u = xf(y)$, $v = v(y)$:

Continuity

$$\rho f + \frac{dv}{dy} = 0 \tag{1}$$

Radial Momentum

$$\rho f^2 + \rho v \frac{df}{dy} + J = \frac{\mu d^2 f}{dy^2} \tag{2}$$

$$\frac{1}{x}\frac{dP}{dx} = J = \text{Const} \tag{3}$$

Axial Momentum

$$\frac{dv}{dx} = 0 \tag{4}$$

Species

$$\frac{\rho v dY_k}{dy} + \frac{d}{dy}(\rho Y_k V_{ky}) - \mathring{\omega} W_k = 0 \tag{5}$$

$$k = 1, 2 - n\text{species}$$

Boundary conditions: $f = 0$ at $y = \pm L$

where

Y_k = mass fraction of the kth species
P = pressure
u, v = tangential and transverse components of the velocity, respectively
ρ = mass density
W_k = molecular weight of the kth species
$\mathring{\omega}$ = molar rate of production of species of the kth species per unit volume
μ = viscosity of the mixture
V_{ky} = diffusion velocity of the kth species in the Y direction

The molar production rates were obtained from a hydrogen/oxygen chemistry mechanism containing eight species and 18 elementary reactions (Warnatz, 1984). Due to heat losses in the reactor that could not be easily quantified, the energy equation was not solved; rather, our experimental temperature profiles were used as a solution to the energy equation in the simulation. The solution to these equations provides a time-temperature history for the fluid carrying the particles.

Because of the presence of steep temperature gradients, the residence time of particles is considerably altered from that of the mean gas flow due to the thermophoretic effect. Thermophoresis is particularly important near the stagnation plane where the fluid velocity is low and where thermophoretic velocities are on the order of the convective velocity. An estimate of the thermophoretic velocity assuming free molecular flow was obtained at each point in the flow field by the following expression (Talbot et al., 1980).

$$V_{Th} = -0.55\nu \frac{d \ln T}{dy} \tag{6}$$

where V_{Th} is the thermophoretic velocity, T is the temperature, and ν is the kinematic viscosity. In some of the flames studied, the thermophoretic effect was large enough to increase the residence time of particles by a factor of two.

Our previous experimental results indicated that the concentration of oxygen was not a significant factor on the yield of particles and that particle initiation took place at sufficiently high temperatures to suggest that silane pyrolysis would play an important role. Furthermore, simulations of silane conversion to silicon have shown the rate-limiting step to be the unimolecular decomposition of silane (Coltrin et al., 1984). The monomer production rate was, therefore, calculated by assuming that the rate-limiting step to the production of SiO_2 is the unimolecular decomposition of silane, as a result of the high activation energy of this step.

$$SiH_4 \xrightarrow{k_1} SiH_2$$

$$SiH_2 \xrightarrow{k_2} SiO_2$$

$$k = 5.2 \times 10^{+12} (\exp - 52{,}000/\mathrm{RT})\ 1/\mathrm{s}]$$

$$k_2 = \text{instantaneous}$$

Particle Growth Models

In order to obtain a better understanding of the dynamics of ceramic particle formation and growth it is necessary to develop phenomenological models for these processes. The models should allow for consumption of the precursor, nucleation of the refractory from the gas phase, and subsequent growth by surface condensation and coalescence. Classical theories of homogeneous nucleation (Zettlemoyer, 1969) constrain the nucleation rate through the supersaturation, as expressed by a balance between the bulk and surface free energies. However, when dealing with materials with low vapor pressure, high degrees of supersaturation exist even at flame temperatures; the surface free energy constraint may be neglected. Under this assumption, the formation rate of the condensed species will be determined by kinetic rather than thermodynamic considerations. The rates of collisions in the free molecular regime are very well known and can be applied to the collisions between molecules, molecules and clusters, molecules and particles and particles, etc. This type of formalism does not distinguish the processes of homogeneous nucleation, surface growth, and coalescence, but treats them as simple collision processes which can be well described by kinetic theory.

This kinetic approach suggests using the aerosol dynamic equation (ADE) used for the simulation of coagulation, as a starting point.

$$\frac{dN_i}{dt} = \frac{1}{2}\sum_{j=1}^{i-1} \beta_{j,i-j} N_j N_{i-j} - N_i \sum_{j=1}^{\infty} \beta_{ij} N_j \tag{7}$$

where N_i is the number density of colliders (molecules, clusters, and particles) of size i, and β is the collision coefficient. The equation relates to the net rate of change in the number density of particle size i by collision processes. If all particles are in the free molecular regime, the collision coefficients β_{ij} are given by kinetic theory:

$$\beta_{ij} = \left(\frac{3}{4\pi}\right)^{1/6} \left(\frac{6kT}{\rho_p}\right)^{1/2} \left(\frac{1}{U_i} + \frac{1}{U_j}\right)^{1/2} (U_i^{1/3} + U_j^{1/3})^2 \tag{8}$$

where k is the Boltzmann constant, T is the temperature, ρ_p is the collider mass density, and U_i and U_j are the respective volumes of the colliding species. Implicit in this assumption is that all colliders (molecules, clusters, and particles) will have mass densities corresponding to the bulk material.

Because of the size range, over which growth occurs (angstroms to micrometers), bookkeeping is the limitation in a computer simulation. This problem can be surmounted by two different approaches which have been developed for the simulation of coagulating aerosols. Dobbins and Mulholland (1984) assumed that the particle-size distribution of aerosols undergoing coagulation was log-normal. This allowed them to solve for the

moments of the aerosol dynamic equation (ADE) for coagulation of soot particles. Alternatively, one can sectionalize the particle-size domain and integrate the ADE between domains, as developed by Gelbard et al. (1980) for coagulation of aerosols. Under the conditions of high supersaturation, both of these approaches should in principle be extendable to account for nucleation and surface growth in addition to coagulation. Wu et al. (1987) have used a discrete-sectional representation of the ADE, a modification of Gelbard et al. (1980), for the simulation of silicon particles in a heated flow reactor. Their particle-size measurements, which were conducted at the exit of the reactor, showed good agreement with the predictions of the model.

Moment Method Solution

The starting point for this method is the continuum representation of the ADE, including a source term for the monomer (SiO_2) formation rate, R_m.

$$\frac{dN(v,t)}{dt} = -N(v,t)\int_j^\infty \beta(v,u)\,N(u,t)\,du + \frac{1}{2}\int_j^v \beta(u,v-u)\,N(u,t)\,N(v-u,t)\,du + R_m \quad (9)$$

For the coagulation of aerosols, it is widely accepted that the distribution of particle sizes can be accurately represented as log-normal.

$$N(v,t) = \frac{N}{v}\frac{1}{\sqrt{2\pi}\sigma_v(t)}\exp\left\{-\frac{1}{2}\left(\ln\frac{v/v_g(t)}{\sigma_v(t)}\right)^2\right\} \quad (10)$$

where v_g and σ_v are the unknown time-dependent geometric mean volume and mean standard deviation, respectively. In this study, we are assuming that a log-normal distribution is applicable to a range of colliders which span from molecules to particles. The validity and effect of this assumption will in part determine the feasibility of using such a model. In order to obtain a solution to the ADE, moments of the equation are taken.

$$\frac{dM_o}{dt} = -\frac{1}{2}\int_0^\infty\int_0^\infty \cdot \beta(v,u)N(v,t)N(u,t)\,dv\,du + R_m(t) \quad (11)$$

$$\frac{dM_1}{dt} = R_m(t)v_m \quad (12)$$

$$\frac{dM_2}{dt} = \int_0^\infty\int_0^\infty \cdot vu\beta(v,u)N(v,t)N(u,t)\,dv\,du + R_m(t)v_m^2 \quad (13)$$

The ADE has been expressed in terms of its first three moments, which have particular significance to this problem. The zeroth moment (M_o) is simply N, the number density of colliders. The first term expresses the decrease in number density of particles resulting from collision. This is balanced by the rate, at which new particles (monomers) are formed by chemical reaction. The first moment (M_1) is the number density times the particle volume, which gives the volume fraction (ϕ). Since new mass to the system is introduced only through the formation of monomer as a result of chemical reaction, the time rate of change of the first moment is simply equal to the monomer formation rate times the volume (v_m) of the monomer. The second moment adds closure to the problem and is proportional to our experimental measurement of the optical scattering power. Finally, the mean volume (v_g) and the standard deviation (σ_v) are related to the first three moments by:

$$v_g = \frac{\phi^2}{N^{3/2}M_2^{1/2}} \quad (14)$$

$$\sigma_v^2 = \ln\left\{\frac{M_2N}{\phi^2}\right\} \quad (15)$$

Polynomial fits to the double integrals are obtained from the work of Dobbins and Mulholland (1984), which result in three ordinary differential equations for the particle field,

$$\frac{d(No)}{dt} = -2\left(\frac{3}{4\pi}\right)^{1/6}\left(\frac{12kT}{\rho_p}\right)^{1/2}\rho No^2\left[\frac{\phi o^2}{No^{3/2}M_2o^{1/2}}\right]^{1/6} \cdot \exp\left[\frac{3}{16}\ln\frac{M_2oNo}{\phi o^2}\right] + R_m(t) \quad (16)$$

$$\frac{d(\phi o)}{dt} = R_m(t)v_m \quad (17)$$

$$\frac{d(M_2o)}{dt} = 4\left(\frac{3}{4\pi}\right)^{1/6}\left(\frac{12kT}{\rho_p}\right)^{1/2}\rho No^2\left[\frac{\phi o^2}{No^{3/2}M_2o^{1/2}}\right]^{3/16} \cdot \exp\left[\frac{65}{48}\ln\frac{M_2oNo}{\phi o^2}\right] + R_m(t)v_m^2 \quad (18)$$

The independent variables (N, ϕ, and M_2) have been expressed in density-normalized variables; $No = N/\rho$, $\phi = \phi/\rho$ and $M_2o = M_2/\rho$ in order to correct for density changes due to the temperature profile. These equations were solved simultaneously using the time temperature history and source rates as discussed in the previous section.

Sectional Model Solution

An advantage of the method of moments is that it is computationally simple. However, this is obtained at the expense of assuming that the particle-size distribution can always be described as log-normal. To check the validity of this assumption it is desirable to compare the result with a model where this assumption is not imposed. The sectional representation relies on dividing the particle field into sections (bins), from which material is transferred by varous inter- and intrasectional collision processes. The MAEROS representation of the problem developed for the coagulation of aerosol particles by Gelbard and Seinfeld (1980) was used over a size domain of 4.4 Å to 1.6 μm, using 35 sections.

Results and Discussion

Mean properties

The nucleation and growth models described above allow the calculation of particle size, number density, and size distribution as a function of time (or distance). These can now be applied to

conditions used in our experiments. In particular, a rigorous test of the capabilities and limitations of the models require that a wide range of experimental conditions be compared. The simulations were performed for two flame conditions, in which temperature was the independent measured variable; temperature profiles for these two flames are presented in Figure 3 in terms of residence time to the stagnation point and labeled flame 1 and 2 for convenience.

Figure 4 is a plot of number density vs. residence time in flame 1 for a silane concentration of 0.365 mol % in the hydrogen stream (see Figure 1), in which curves *a* and *b* correspond to the results obtained with the moment and sectional models, respectively. The results from both models agree quite well in all portions of the particle field. During the initiation phase, the number density (i.e., sum of all molecules, clusters and particles) increases to a maximum of 6.0×10^{13} at 35 ms, corresponding to the location of maximum monomer production rate. Subsequently, as the silane is depleted, there is a rapid transition to a lower number density as the molecules and clusters are collisionally scavenged. The remainder of the process is one of particle consolidation. The experimentally-observed number density by contrast shows a vastly different shape during the particle forming stage. The reason for this discrepancy results from the difference between what the simulation views as particles and what the diagnostic views as particles. The simplicity in the simulation was obtained at the expense of not distinguishing molecules, clusters and particles, which was particularly important in the construction of the moment method solution. However, from an experimental viewpoint, particles are, barring an exact scientific definition of particles, those that can be resolved by a diagnostic.

The diagnostic technique used relied on Mie scattering, which defines the lower size limit for which one can size a particle. For the wavelength of 514.5 nm (Ar-ion green line) used in the experiment, the lower limit of observability is on the order of 40 nm. We can reinterpret the simulation results by counting particles larger than 40 nm in the sectional representation, resulting in curve *c*. This reinterpretation in the bookkeeping provides a much more reasonable view of what the experiment actually measures. In particular, the steep ascent in number density seen in the simulation as compared to the experiment provides a temporal comparison of the appearance of particles in the window of

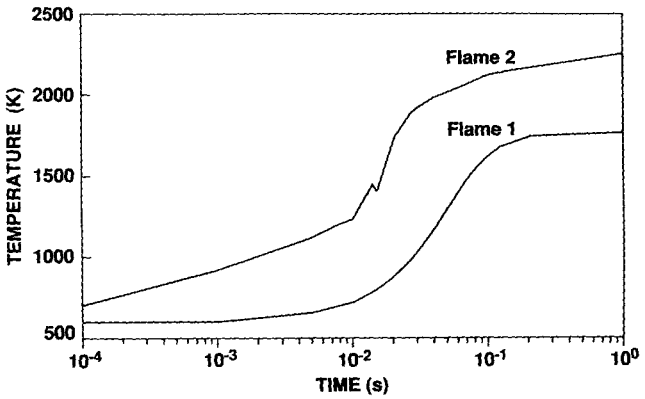

Figure 3. Temperature profiles for flame 1 and 2.
Flame 1: $H_2/O_2/Ar$ mole fractions = 0.20/0.13/0.67
Flame 2: $H_2/O_2/Ar$ mole fractions = 0.34/0.25/0.41

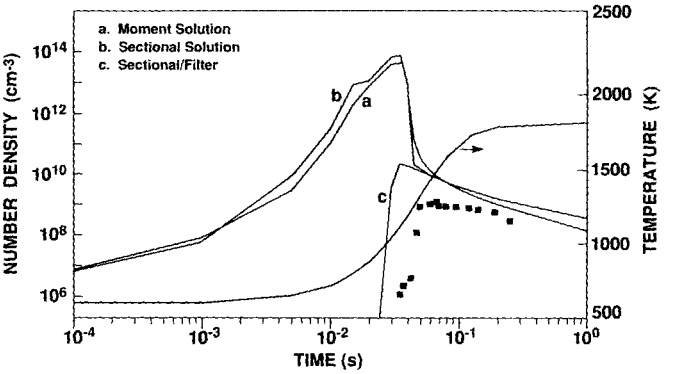

Figure 4. Number density vs. residence time in flame 1.
Curve *a*, moment method solution
Curve *b*, sectional method solution
Curve *c*, sectional solution with 40 nm cutoff
Open squares, experimental measurements
Silane mole fraction in fuel stream = 0.365%

observability of the experiment, which may be thought of as an apparent pseudonucleation process. The agreement is quite reasonable as the simulation predicts the pseudonucleation within 15 ms. The number density is overpredicted, particularly early on, although the experimental and theoretical curves are in better agreement at later times. The fact that the number densities do not coincide with the experimental values is not so disturbing, since the number density has the largest measurement uncertainty (Zachariah et al., 1989).

In the simulations, mass is conserved: i.e., all silicon introduced as silane forms SiO_2. In the experiment, however, volume fraction measurements calculated from the product of average particle volume and number density yield a 50% shortfall in silicon atoms. It is unlikely that significant amounts of silicon (in any chemical form) remains in the gas phase, suggesting a shortfall in the diagnostic. This could be attributed to the measurement of the number density, when one considers that particle number density is calculated from the measured diameter and the scattering intensity. Since scattering intensity in the near Raleigh regime is proportional to the diameter to the sixth

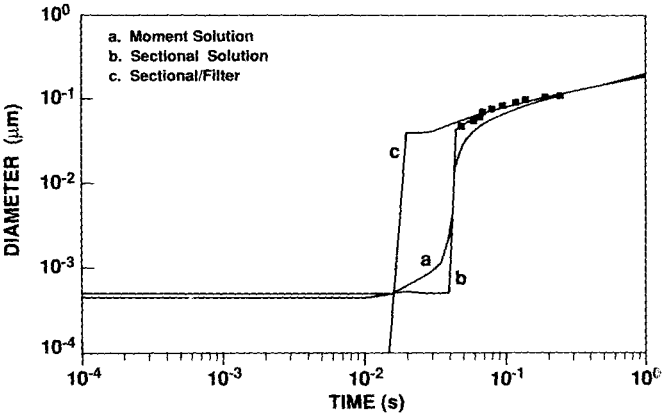

Figure 5. Particle diameter vs. residence time in flame 1.
Curve *a*, moment method solution
Curve *b*, sectional method solution
Curve *c*, sectional solution with 40 nm cutoff
Open squares, experimental measurements
Silane mole fraction in fuel stream = 0.365%

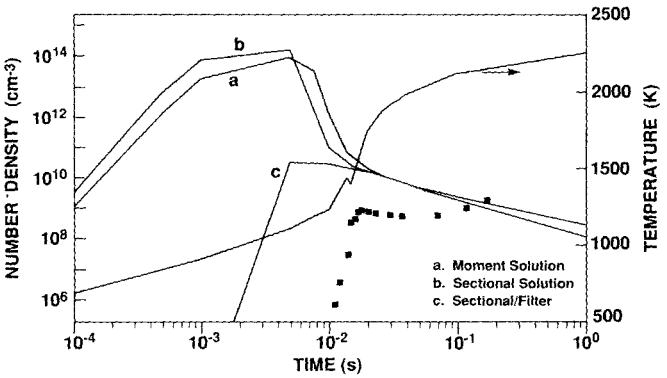

Figure 6. Number density vs. residence time in flame 2.

Curve *a*, moment method solution
Curve *b*, sectional method solution
Curve *c*, sectional solution with 40 nm cutoff
Open squares, experimental measurements
Silane mole fraction in fuel stream = 0.38%

power, a 10% error in the measured particle size yields 77% error in number density.

The measured and calculated particle diameters are shown in Figure 5 for flame 1. Curves *a* and *b* both show a steep rise in particle size around 40 ms which corresponds to the sharp drop in particle number density. The sharp rise results not from sudden particle growth, but rather from the rapid decay of the monomer source rate from a peak of $5 \times 10^{18}/\text{cm}^{-3} \cdot \text{s}^{-1}$ at 35 ms down to $5 \times 0^{11}\ \text{cm}^{-3} \cdot \text{s}^{-1}$ at 45 ms.

By including the numerical particle filter, curve *c* is generated in an analogous manner to that of number density in Figure 4. The measured particle sizes compare quite favorably with the prediction, although they do not extend as far back in time as does curve *c*, similar to the number density observations. The results for number density and particle size for a higher-temperature flame (flame 2) are illustrated in Figures 6 and 7. In comparing the results from the two flames, the most noticeable effect is acceleration of the chemical kinetics in flame 2 resulting form the higher temperature, which in turn accelerates particle production. The peak in monomer production occurs at 5

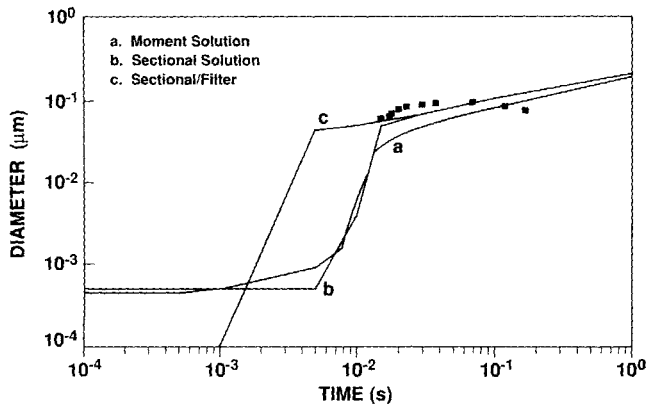

Figure 7. Particle diameter vs. residence time in flame 2.

Curve *a*, moment method solution
Curve *b*, sectional method solution
Curve *c*, sectional solution with 40 nm cutoff
Open squares, experimental measurements
Silane mole fraction in fuel stream = 0.38%

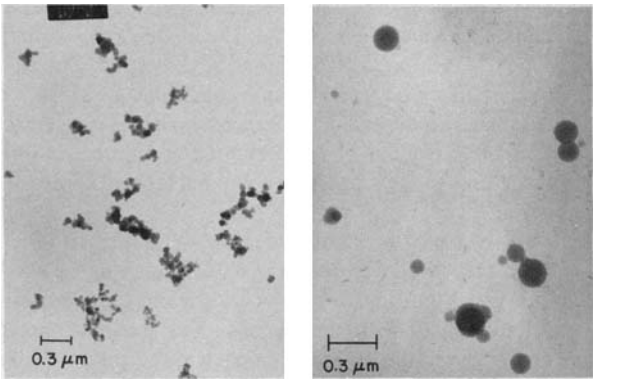

Figure 8. Transmission electron micrographs of silica particles before and after *in-situ* temperature-induced sintering.

ms ($2.0 \times 0^{19}/\text{cm}^3 \cdot \text{s}$), which as in the cooler flame, corresponds to the peak in number density. The temporal comparison of the "pseudonucleation" show similar results to the cooler flame, with particle appearance predicted to occur about 8 ms ahead of the experimental observations.

The most noticeable discrepancy between the model and experiment occurs at about 40 ms, where an increase in the experimental particle number density is observed with a corresponding decrease in particle size. This turns out to be an extremely important result with regard to particle synthesis, although beyond the scope of either model. The observed effects we believe arise from particle sintering due to the elevated temperatures of this flame. When particles which are agglomerates flow into a high-temperature region, surface forces begin to compete with the declining viscous forces resulting in flow of the glass in order to reduce its surface area. In addition, we believe, loosely attached primary particles might become dislodged, creating new particles (as evidenced by the increasing number density near the stagnation plane). The overall result is the production of highly spherical particles as shown in Figure 8. From the standpoint of materials synthesis, this is a highly desirable effect; *in-situ* sintering could in principle be used to produce the appropriate particle morphology. From the standpoint of modeling the process, incorporation of a sintering mechanism and particle morphology would greatly add to the complexity of a simulation.

Finally, simulations are shown for experiments conducted at lower silane concentrations. Figures 9 and 10 illustrate the particle growth in flame 1 when silane concentration is reduced by a factor of ten (to 0.035 mol % in fuel stream). In all cases of extremely-low silane loading, the models showed much earlier pseudonucleation at much higher number densities than was observed. Particle size was consistently underpredicted in all the flames studied with low silane concentration. The most obvious conclusion is that the delay in particle formation is a supersaturation effect and therefore not kinetically-controlled; however, this is not a reasonable explanation for materials of this class, which have extremely low vapor pressures at these temperatures. An alternate possibility is that, under low silane concentration, the rate-limiting source for production of SiO_2 is not the pyrolysis of silane as has been assumed. This is perhaps a more satisfying explanation although not particularly helpful, as it suggests that a more comprehensive mechanism is necessary in

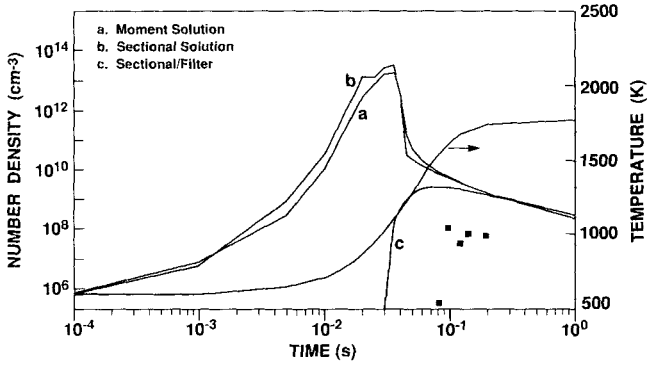

Figure 9. Number density vs. residence time in flame 1.

Curve *a*, moment method solution
Curve *b*, sectional method solution
Curve *c*, sectional solution with 40 nm cutoff
Open squares, experimental measurements
Silane mole fraction in fuel stream = 0.038%

order to account for silica formation under a variety of conditions.

Recent experiments have provided some evidence regarding chemical kinetic effects on particle nucleation (Zachariah and Semerjian, in press). In particular it was observed that laser attenuation (514.5 mm) far in excess of that explainable by simple scattering was observed in flames with high silane loading. Being a dielectric, SiO_2 has no imaginary part of the refractive index at visible wavelengths, which suggests that something other than SiO_2 at least initially formed. The most likely explanation is that, at the higher concentrations of silane used, pyrolysis is indeed the important process, as was first suggested in the model. But, rather than oxidizing immediately, the clusters probably grow as silicon, before being subsequently oxidized (Zachariah and Joklik, 1989). At very low concentrations of silane, no attenuation in the laser was observed, suggesting that the atomic silicon channel was no longer important. It is clear that, in a mixed (reaction-diffusion) control system, an accurate representation of the chemistry is needed in order to appreciate the kinetics of particle formation. Certainly, this would be of particular importance when chemical composition of the particle is of critical importance.

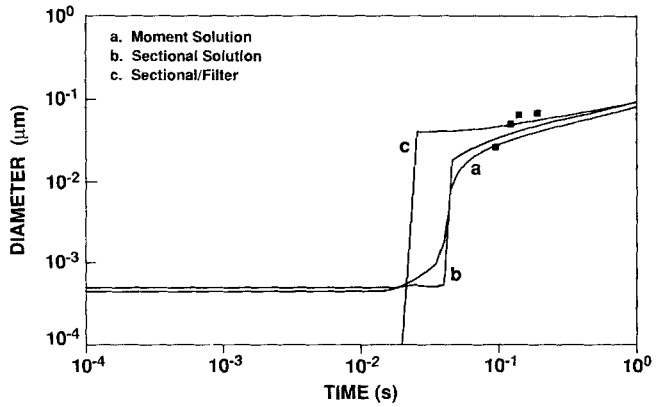

Figure 10. Particle diameter vs. residence time in flame 1.

Curve *a*, moment method solution
Curve *b*, sectional method solution
Curve *c*, sectional solution with 40 nm cutoff
Open squares, experimental measurements
Silane mole fraction in fuel stream = 0.038%

Polydispersity and particle-size distribution effects

Simulations from both of the sectional and moment methods show that the two models compare quite favorable with each other in terms of mean particle size and number density. From a particle synthesis point of view, the size distribution can be as important as the mean size. In particular, one wishes a model to accurately predict the polydispersity as a function of time for reactor design purposes. Indeed, particle morphology (aggregate vs. sphere) is very dependent on the path taken (heterogeneous vs. homogeneous) for gas to particle conversion and therefore intimately involved in the polydispersity.

By definition, the moment method will always be constrained to have a log-normal size distrubution, although its width (polydispersity) will vary with time. The sectional method as previously described has no constraints on the form of the distribution function and as such might be considered to be a more accurate representation. Figure 11 shows plots of particle polydispersity, as expressed by the standard deviation (sigma) from the geometric mean particle diameter as a function of time. The curves in Figure 11 correspond to flame 1 with the labels on the curves as previously described. It is clear that there are marked differences between the two methods. All three curves show convergence to the self-preserving size distribution as expected. Indeed, the experimental data reduction method is validated, since a self-preserving size distribution was assumed in the Mie scattering calculations. However, the route to the self-preserving distribution clearly takes different paths. In particular, the moment method (curve *a*) shows a peak in the polydispersity at almost the same point that the sectional solution (curve *b*) shows a minimum. The discrepancy can be followed by tracking the sectional method as being the more nearly-correct solution.

During the initial stages of cluster-particle formation, the monomer production rate is relatively low ($R_m < 1 \times 10^{16}$ cm$^{-3} \cdot$ s^{-1} at time < 2 ms) such that the processes leading to clusters also lead to an increase in the particle-size distribution. As the source rate increases, as a result of increasing temperature, to a peak of 5×10^{18} cm$^{-3} \cdot$ s^{-1} the polydispersity reaches a minimum at about 35 ms. This results from the inability of processes subsequent to monomer production to control the monomer and dimer concentrations. As the monomer concentration is so high, the mean size and polydispersity are dominated primarily by the monomer. Indeed, dur-

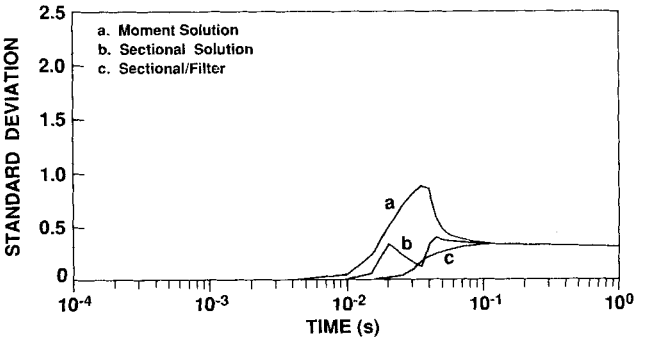

Figure 11. Log of the standard deviation of particle diameter in flame 1.

Curve *a*, moment method solution
Curve *b*, sectional method solution
Curve *c*, sectional solution with 40 nm cutoff
Open squares, experimental measurements
Silane mole fraction in fuel stream = 0.365%

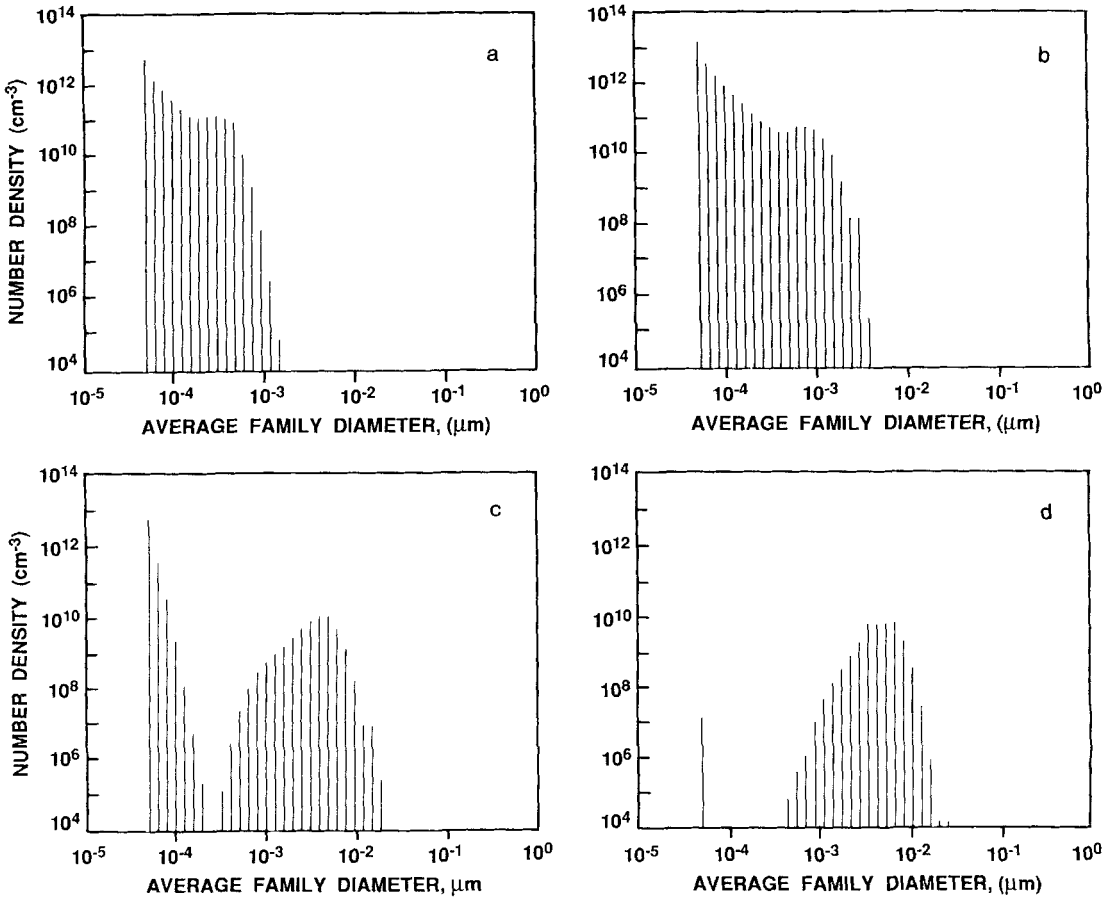

Figure 12. Number density vs. particle diameter calculated from the sectional model for flame 1.
a, 20 ms; *b*, 25 ms; *c*, 40 ms; *d*, 45 ms

ing this phase the mean size of the clusters may actually decrease! As the monomer source begins to decrease as a result of depleation of the precursor, the polydispersity begins a near monotonic rise to its eventual self-preserving asymptote. Figure 12 plots the corresponding size distribution as calculated from the sectional method for 20, 25, 40 and 45 ms. It is clear that the high monomer formation rates play havoc with the assumption of a log-normal size distribution and is the reason for the discrepancy between the moment and sectional model.

The polydispersity observed for the higher-temperature flame is shown in Figure 13. Like the cooler flame, the disparity between the two methods is quite evident, but also quite different from that of the cooler flame. In particular, the sectional method shows a very sharp spike and no observed minimum. The differences may again be attributed to the competition between the monomer production rate and the subsequent processes leading to larger particles. In the case of the hotter flame, the polydispersity is kept low as a result of the high monomer source rate, which keeps the monomer concentration high. As the precursor concentration declines, with it the monomer source rate a bimodal distribution develops and thus results in the spike in the standard deviation. This can be seen in Figure 14 which illustrates the evolution of the particle-size distribution. As in the case of the cooler flame, the particle-size distribution is clearly not log-normal during the early stages of particle formation.

Summary and Conclusions

Two methods to describe particle formation and growth have been proposed to describe the formation of silica particles in flames. The models are based on the assumption that molecules,

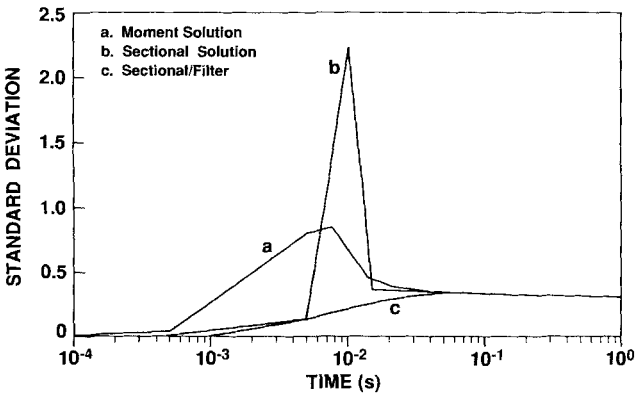

Figure 13. Log of the standard deviation of particle diameter in flame 2.
Curve *a*, moment method solution
Curve *b*, sectional method solution
Curve *c*, sectional solution with 40 nm cutoff
Open squares, experimental measurements
Silane mole fraction in fuel stream = 0.38%

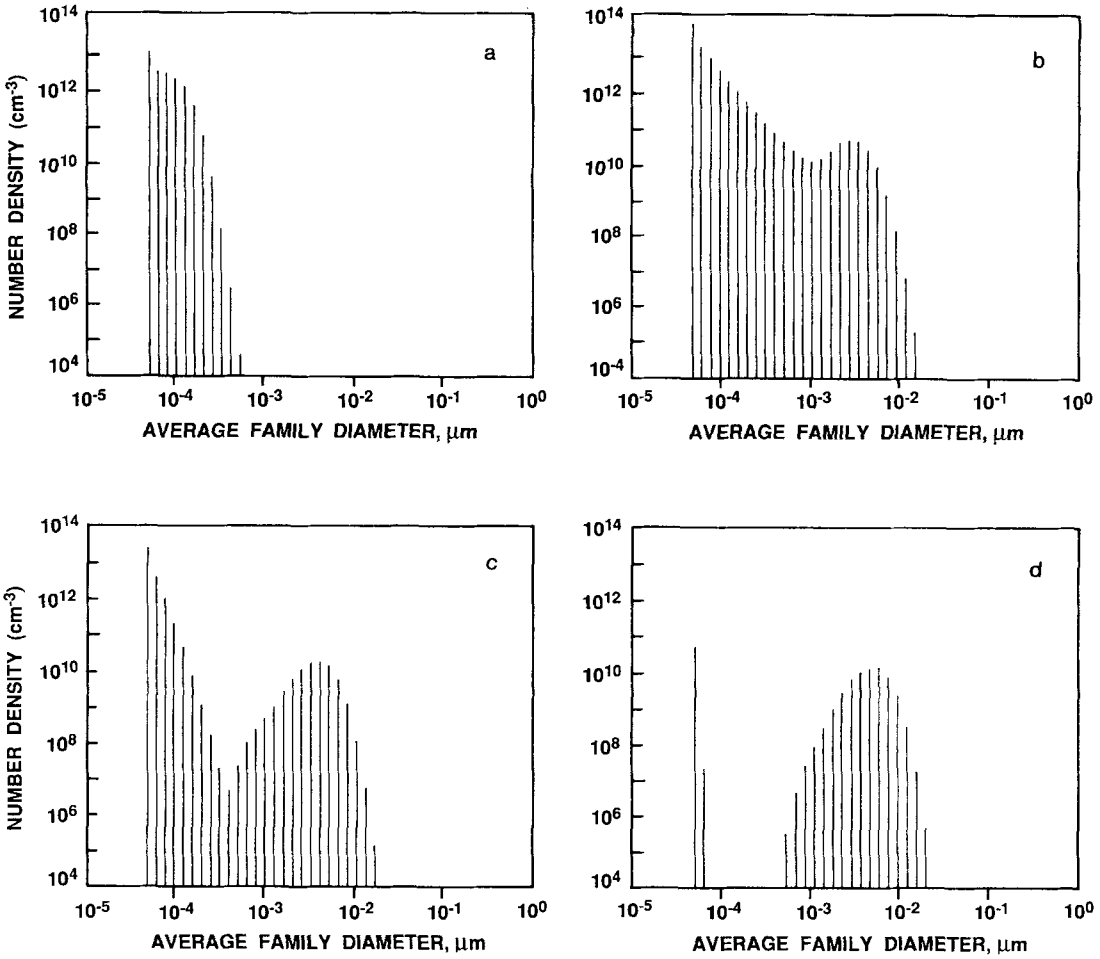

Figure 14. Number density vs. particle diameter calculated from the sectional model for flame 2.
a, 1 ms; *b*, 5 ms; *c*, 8 ms; *d*, 10 ms

clusters, and particles have the same physical properties and that there exists no free energy barrier to nucleation. This leads to a purely kinetic description for all phases of particle formation. A reacting flow model for a counterpropagating diffusion flame was used to generate a time-temperature history, from which the particle models were integrated. The moment and sectional models were found to yield similar results for mean particle properties (size and number density). *In-situ* laser scattering measurements were used to determine particle size and number density in a counterflow geometry and compared to the model predictions. The conclusions reached as applied to silica formation were that agreement between the theory and experiment were extremely good under conditions of high silane concentration, but that at very low silane concentrations the models were unable to predict the number and location of particle formation. The results suggest that a more comprehensive chemical mechanism is required in order to describe particle formation under all conditions.

While agreement between the two models was particularly good for prediction of mean properties (particle size and number density), the moment model was unable to describe the evolution of the particle-size distribution. Had the particle-size distribution varied from the log-normal for an extended period, as might be for the case of a continuously-reinforced reactor, the agreement between the two models would undoubtedly become progressively worse. From the standpoint of computational ease, however, the method of moments provides a simple means of obtaining reasonable results.

Acknowledgment

The authors wish to acknowledge the valuable help and advice of Dr. Mitch Smooke (Yale University) regarding the modeling of counterflow diffusion flames.

Literature Cited

Alam, M. K., and R. C. Flagan, "Controlled Nucleation Aerosol Reactors: Production of Bulk Silicon, *Aerosol Sci. Tech.*, **5**, 237, (1986).

Cannon, W. R., S. C. Danforth, J. S. Haggerty, and R. A. Marra, "Sinterable Ceramics Powders from Laser-Driven Reactions: II Powder Characteristics and Process Variables," *J. Amer. Ceram. Soc.*, **65**, 330 (1982)

Chung, S. L., and J. L. Katz, "The Counter Flow Diffusion Flame Burner: A New Tool for the Study of Nucleation of Refractory Compounds," *Combust. Flame*, **61**, 271 (1985).

Coltrin, M. E., R. J. Kee, and J. A. Miller. "A Mathematical Model of Coupled Fluid Mechanics and Chemical Kinetics in a Chemical Vapor Deposition Reactor," *J. Electrochem. Soc*, **131.**, 425 (1984).

Dobbins, R. A., and G. W. Mulholland, "Interpretation of Optical Measurements of Flame Generated Particles," *Combust. Sci. Technol.*, **40,** 175 (1984).
Gelbard, F., Y. Tambour, and J. H. Seinfeld, "Sectional Representation for Simulating Aerosol Dynamics," *J. Coll. Interf. Sci.*, **76,** 541 (1980).
Girshick, S. L., C. Chiu, and P. H. McMurry, "Modeling Particle Formation and Growth in a Plasma Synthesis Reactor," *Plasma Chem. and Plasma Process.*, **8,** 145 (1988).
Sanders, H. J., "High-Tech Ceramics," *Chem. Eng. News* (July 9, 1984).
Smooke, M. D., I. K. Puri, and K. Seshadri, "A Comparison Between Numerical Calculations and Experimental Measurements of the Structure of a Counterflow Diffusion Flame Burning Diluted Methane in Diluted Air," *Int. Symp. on Combustion,* 1783 (1986).
Talbot, L., R. K. Cheng, R. W. Schefer, and D. R. Willis, "Thermophoresis of Particles in a Heated Boundary Layer," *J. Fluid Mech.*, **101,** 737 (1980).
Ulrich, G. D., and N. S. Subranmanian, "Particle Growth in Flames III. Coalescence as a Rate-Controlling Process," *Combust. Sci. Technol.*, **17,** 119 (1977).
Ulrich, G. D., "Flame Synthesis of Fine Particles," *Chem. Eng. News,* (Aug. 6, 1984).
Warnatz, J., "Rate Coefficients in the C/H/O System," *Combustion Chemistry,* ed., W. C. Gardiner, Springer-Verlag (1984).
Wu, J. J., H. V. Nguyen, and R. C. Flagan, "A Method for the Synthesis of Submicron Powders," *Langmuir,* **3,** 266 (1987).
Zachariah, M. R., D. Chin, J. L. Katz, and H. G. Semerjian, "Dynamic Light Scattering and Angular Dissymmetry for the In-Situ Measurement of Silicon Dioxide Particle Synthesis in Flames," *Appl. Optics,* **28,** 530 (1989).
———, "Silica Particle Synthesis is a Counter Flow Diffusion Flame Reactor," *Combust. Flame* (in press).
Zachariah, M. R., and H. G. Semerjian, "Experimental and Numerical Studies of Refractory Particle Formation," *J. of High Temp. Sci.* (in press).
Zettlemoyer, A. C., *Nucleation,* Marcel Dekker, New York (1969).

Manuscript received June 14, 1989, and revision received Sept. 15, 1989.